Biosensors and Bioelectronics 26 (2011) 4320–4325

Contents lists available at ScienceDirect

Biosensors and Bioelectronics

journal homepage: www.elsevier.com/locate/bios

Methyl parathion hydrolase based nanocomposite biosensors for highly sensitive and selective determination of methyl parathion

Shizhen Chen[a], Jing Huang[a], Dan Du[a], Jinlin Li[b], Haiyang Tu[a], Deli Liu[a], Aidong Zhang[a,*]

[a] Key Laboratory of Pesticide & Chemical Biology of Ministry of Education, Chemistry College, Central China Normal University, Luoyu Str. 152, Wuhan 430079, Hubei Province, PR China
[b] Key Laboratory of Catalysis and Materials Science of the State Ethnic Affairs Commision & Ministry of Education, South-Central University for Nationalities, Wuhan 430074, PR China

ARTICLE INFO

Article history:
Received 4 March 2011
Received in revised form 11 April 2011
Accepted 12 April 2011
Available online 20 April 2011

Keywords:
Silica sphere
Gold nanoparticle
Multiwall carbon nanotube
Nanocomposite biosensor
Methyl parathion hydrolase

ABSTRACT

This article reports the fabrication of a nanocomposite biosensor for the sensitive and specific detection of methyl parathion. The nanocomposite sensing film was prepared via the formation of gold nanoparticles on silica particles, mixing with multiwall carbon nanotubes and subsequent covalent immobilization of methyl parathion hydrolase. The composite of the individual materials was finely tuned to offer the sensing film with high specific surface area and high conductivity. A significant synergistic effect of nanocomposites on the biosensor performance was observed in biosensing methyl parathion. The square wave voltammetric responses displayed well defined peaks, linearly proportional to the concentrations of methyl parathion in the range from 0.001 $\mu g\,mL^{-1}$ to 5.0 $\mu g\,mL^{-1}$ with a detection limit of 0.3 $ng\,mL^{-1}$. The application of this biosensor in the analysis of spiked garlic samples was also evaluated. The proposed protocol can be used as a platform for the simple and fast construction of biosensors with good performance for the determination of enzyme-specific electroactive species.

1. Introduction

Methyl parathion hydrolase (MPH) is one member of the organophosphorus hydrolase family, which has been found in several bacteria capable of specific degradation of methyl parathion (Cui et al., 2001; Mulbry and Karns, 1989). The MPH specific substrate, methyl parathion, is still widely used as a potent insecticide and acaricide in agriculture. Since its high toxicity towards various organisms (Kumar et al., 2006), developing simple, fast and sensitive methods by using MPH for the specific determination of methyl parathion is of great interest in environmental and food safety concerns. The MPH catalytic hydrolysis of methyl parathion produces dimethyl phosphate and 4-nitrophenol with a high turnover rate (Grimsley et al., 2005), and the later is an electroactive compound (Hu et al., 2001) that makes the construction of an amperometric biosensor possible.

The conventional acetylcholinesterase (AChE) biosensors with different fabrication methodologies have been extensively explored for the determination of methyl parathion (Dzyadevych et al., 2002; Villatte et al., 2002). This kind of biosensors were based on the irreversible inhibitory effect of methyl parathion towards the AChE, and expected to be used in a disposable fashion. Recently, several members of organophosphorus hydrolase family other than MPH, immobilized on the nanocomposite supports such as graphene/Nafion nanohybrid matrix (Choi et al., 2010), single-wall carbon nanotube Pedrosa et al., 2010), and mesoporous carbon/carbon black (Lee et al., 2010), have been reported as the biosensing components for the determination of organophosphorus chemicals with molecular structures analogous to methyl parathion. For the selective and sensitive determination of methyl parathion, an MPH biosensor was described by utilizing the nanocomposite of CdTe quantum dots/carbon nanotube/Au nanoparticles (Du et al., 2010).

Nanocomposite based amperometric biosensors capable of determining the in situ generated enzymatic product(s) of electroactivity should satisfy several fundamental requirements in the elaboration of biosensing membranes. Enzyme loading, mass transportability, charge conductivity, biocompatibility, and reproducibility are the mostly concerned factors in fabrication of such nanocomposites (Bakker and Qin, 2006). Taking the advantages of large specific surface area, good conductivity, and other merits of nanocomposites, nanocomposite biosensors usually possess enhanced biosensor performances (Li et al., 2009; Pividori and Alegret, 2010; Su et al., 2010). Since the complexity of the multiple components in nanocomposites, the contributions of the individual components should be comprehensively weighted. Thereby the optimization of the composition and control of the nanocomposite

* Corresponding author. Tel.: +86 27 67867635.
E-mail address: adzhang@mail.ccnu.edu.cn (A. Zhang).

0956-5663/$ – see front matter © 2011 Elsevier B.V. All rights reserved.
doi:10.1016/j.bios.2011.04.025

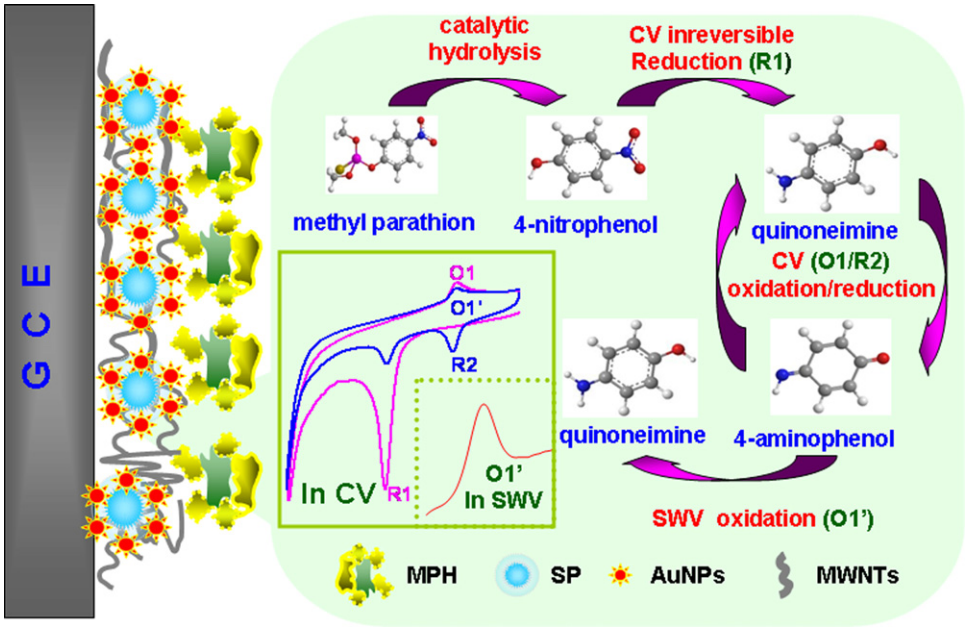

Scheme 1. Working principle of MPH biosensor for determination of methyl parathion.

morphology become an indispensable procedure for constructing a biosensor with good performance.

In this article, a novel nanocomposite interface for immobilizing MPH enzyme is proposed and used for the electrochemically specific and sensitive determination of methyl parathion. The nanocomposite was synthesized via the in situ formation of gold nanoparticles (AuNPs) on silica particles (SPs), mixing with multiwall carbon nanotubes (MWCNTs) and subsequent immobilization of MPH enzyme. Several key factors including the SP sizes and the contents of the nanocomposite components have been optimized for achieving a high biosensor performance. Such nanocomposite consisting of the core–shell type SP/AuNPs with combination of MWCNTs is demonstrated to provide an enhanced synergistic effect on the performance of the MPH enzyme based biosensor. The principle for the biosensing methyl parathion is shown in Scheme 1, where the MPH catalyzes the hydrolysis of methyl parathion to release the electroactive 4-nitrophenol, subsequently reduced to 4-aminophenol (R1 and R2 stages) and re-oxidized to quinoneimine (O1 stage) via the voltammteric cycles (CV). The cycle can be stopped at the negative scan end (R2 stage), and the square wave voltammetry (SWV) is then performed via a positive scan to produce quinoneimine (O1′ stage) with a much stronger sensitivity. The mechanism involved in the CV process has been delineated (Alizadeh et al., 2009) and will be discussed later.

2. Materials and methods

2.1. Reagents

Methyl parathion, 3-aminopropyltrimethoxysilane (APTS), tetraethoxysilane (TEOS), N-hydroxysuccinimide (NHS) and 1-ethyl-3-(3-dimethylaminopropyl) carbodiimide hydrochloride (EDC) were purchased from Sigma. Chloroauric acid ($AuCl_3{\cdot}HCl{\cdot}4H_2O$, Au% > 47.8%) was obtained from Sinophacm Chemical Reagent Co. Ltd. All these reagents were used as received without further purification. Multiwall carbon nanotubes (MWCNTs) were a gift from the Institute of Nanometer Technology, Central China Normal University. Methyl parathion hydrolyase (MPH) was isolated and purified as the previously reported procedure (Du et al., 2010). The electrolyte solution was made by dissolving 0.1056 g $K_4Fe(CN)_6$ and 0.0823 g $K_3Fe(CN)_6$ in 100 mL phosphate buffer solution (PBS, pH 7.0) containing 0.1 M KCl. Sodium citrate, anhydrous ethanol, ammonia solution (5 M), and other reagents used were analytical reagent grade. Aqueous solutions were prepared with double-distilled water.

2.2. Preparation of SP@GNP/CNT nanocomposites

SP spheres were synthesized by following the reported method (Stober et al., 1968). Typically, 156 μL of TEOS was added to 175 μL of 5 M ammonia solution (30 wt%) in 2.5 mL of ethanol and 90 μL of water under stirring to hydrolyze TEOS. After 24 h of stirring, a colloidal solution of SPs with a mean diameter 250 nm was obtained. By varying the applied amounts of ammonia solution as 75 μL, 100 μL and 250 μL, NPs with diameters 50 nm, 110 nm, and 450 nm, respectively, were obtained.

The SPs were functionalized with APTS by a reported method (Hiramatsu and Osterloh, 2003), and then the gold nanoparticles were anchored onto SP surface via a seed-mediated growth method (Kim et al., 2009). The anchoring process involved the formation of gold seeds on the SP surface by adding the APTS functionalized SP suspension to the mixed solution of $HAuCl_4$ and sodium citrate, and the subsequent seed growth by introducing sodium borohydride in sodium citrate solution (Kumar Jena et al., 2006). The AuNPs with a mean diameter of 10 nm formed a continuous shell on the SP core surface. After centrifugation purification, the SP/AuNPs particles were dispersed in water for use.

The MWCNTs was activated by heating at reflux in HNO_3 for 10 h according to the reported method (Azadi et al., 2010), and added to the suspension of SP@AuNPs particles. After thorough sonication, the homogeneous SP@AuNPs/MWCNTs was obtained. The pretreating procedure for MWCNTs produced plenty of carboxyl groups on the surface compatible with the hydrophilic SP@AuNPs particles.

2.3. Preparation of biosensors

Before casting the nanocomposites, the GCE electrode was activated through the alumina polishing and subsequent voltammetric cycling according to the reported procedure (Du et al.,

2007). Then the SP@Au/MWCNTs composite suspension (5 μL) was applied to the GEC and left for 2 h at room temperature leading to a semi-dry state. The modified electrode was washed three times by adding proper amount of double-distilled water and appeared as a homogenous film. The MPH enzyme was covalently immobilized onto the nanocomposite film through the EDC/NHS protocol. Thus the nanocomposite electrode was dipped into a solution containing 20 mg mL^{-1} EDC and 10 mg mL^{-1} NHS for 10 h to activate the carboxyl groups on the nanocomposite surface, then coated with 5.0 μL MPH solutions and incubated at room temperature overnight. After washing with PBS, the as prepared MPH/SP@AuNPs/MWCNTs/GCE biosensor was stored at 4 °C for use.

2.4. Characterization of nanocomposites and biosensors

The morphological images were acquired by using a JEOL-JSM-6700F scanning electron microscope with an accelerated voltage 5.0 kV. The electrochemical characterizations were performed on a CHI 660c electrochemical station (Chenhua, Shanghai, China) with a conventional three electrode system comprising platinum wire as the auxiliary electrode, saturated calomel electrode (SCE) as the reference, and the corresponding modified GCE electrode as the working electrode.

2.5. Interface constitution optimization and sensor performance evaluation

For achieving better biosensor configuration, SPs with varying sizes and different amounts of AuNPs and MWCNTs were used to optimize the nanocomposite formation by measuring the corresponding SWV responses towards methyl parathion at a fixed concentration of 0.1 μg mL^{-1}. The SWV measurements were conducted using the similar electrochemical configuration as described in the characterization section. The maximum response for each variable was chosen as the optimal experimental parameter. Thus the obtained optimal conditions are: SP size, 100 nm; solution volumetric ratio of AuNPs/SP, 1:1; MWCNTs amount, 1.5 μg mL^{-1} in the final solution.

The optimized biosensor was employed for the determination of methyl parathion using the conventional three-electrode system and the SWV method. Methyl parathion with varying concentrations in PBS was measured, and the calibration curve, dynamic range, and lowest detection limit were obtained. The selectivity was tested against the responses towards the analogs of methyl parathion; ethyl parathion and paraoxon, and the interferences from oxygen-containing inorganic ions (PO_4^{3-}, SO_4^{2-}, NO_3^-) in solution were also examined. To further demonstrate the practicality of the proposed method, the biosensor was used to determine the concentrations of methyl parathion in spiked garlic samples, and the standard recovery ratios were calculated. The spiked garlic sample was prepared via a similar reported procedure (Al-Otayk et al., 2008), by adding known amount of methyl parathion into ground garlic, followed by extracting with the mixed solution of water and ethanol (volumetric ratio 1:1).

3. Results and discussion

3.1. SEM characterization

The morphology of a matrix layer has a significant effect on the loading of an enzyme and keeping its activity. High loading of enzymes can be easily achieved in various fluffy nanocomposite layers (Cui et al., 2007; Xian et al., 2006). Fig. 1 shows the morphologies of sequential SPs, SP@AuNPs particles, and SP@AuNPs/MWCNTs nanocomposite. As seen from Fig. 1A, the surface of SP appears to be smooth but easily agglomerated. In Fig. 1B, the SP surface is fully decorated with AuNPs, forming core–shell type SP@AuNPs nanocomposites. As shown in the inset of Fig. 1B,

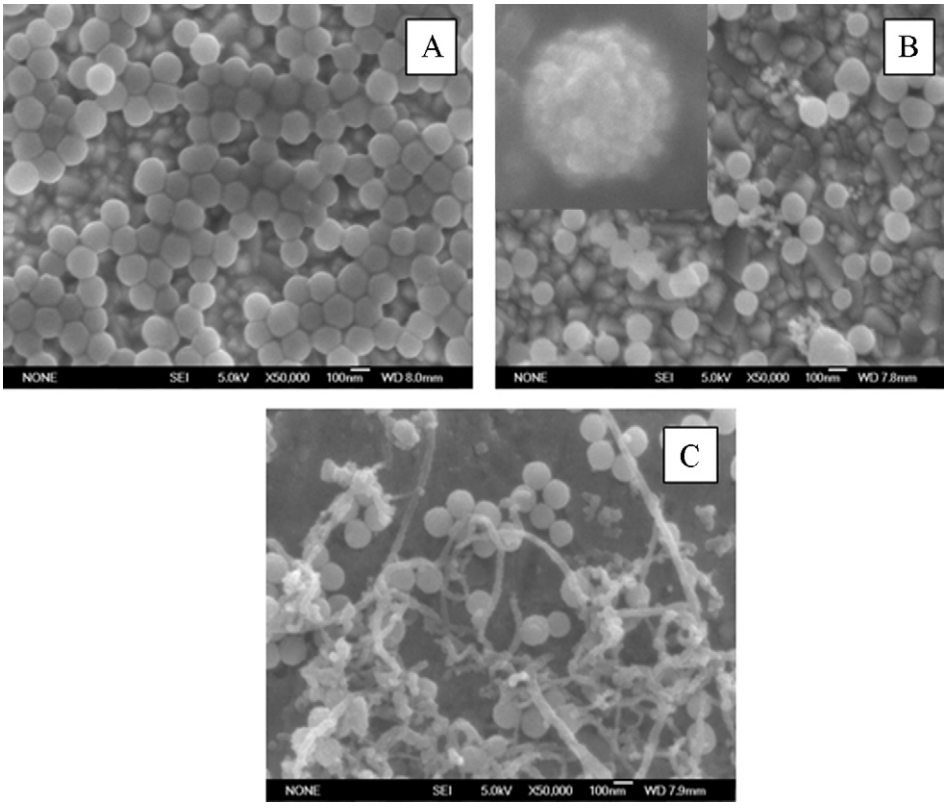

Fig. 1. SEM images of (A) silica sphere, (B) SP@AuNPs core/shell particles, inset: amplified SP@AuNPs core/shell structure, and (C) SP@Au/MWNTs nanocomposite.

many small gold nanoparticles are closely and evenly resided on the surface of the 3-aminopropyl-functionalized SP surface to form a continuous shell. The process of forming gold nanoparticle shell on the core was followed using SEM (data not shown), and a two-step process was revealed. Gold seeds with 2–3 nm in diameter were firstly adsorbed on the surface that supplied numbers of small, randomly oriented crystalline domains for the following seed mediated growth of the Au particles (Zhou et al., 2010). Then the gold seeds began to grow under the reducing condition of sodium borohydride until a continuous shell was selectively formed. The as-made SP@AuNPs core/shell structure with a mean diameter 10 nm can be clearly observed in the inset of Fig. 1B, demonstrating the formation of a highly rough gold nanoparticle shells. In Fig. 1C, the SP@Au/MWNTs nanocomposites displayed a fluffy and network-like structure with a nearly uniform distribution of SP@AuNPs. In the SP@AuNPs/MWCNTs nanocomposite, the surface of the core–shell nanostructure of SP/AuNPs has been functionalized by citrate, whereas the MWCNTs has been pretreated with nitric acid that produce a plenty of carboxyl groups on the surface (Azadi et al., 2010). Thus both of the hydrophilic surfaces exhibit well compatibility, resulting a nearly homogeneous distribution of the two components in the fluffy and network-like structure without obvious agglomeration. This structure is believed to provide a significant increase on the effective electrode area for immobilization of biomolecules. On the other hand, the interparticular force (Vie et al., 2007) and coalescence force (Chen et al., 2004) may render the nanocomposite film enough stability for settling on the surface.

3.2. Electrochemical characterization

The effective electrode areas of GCE electrodes coated with SP@AuNPs and SP@AuNPs/MWCNTs were characterized using cyclic voltammetry, and compared to that of the bare GCE electrode. In the presence of 5 mM $K_3Fe(CN)_6$ in 1 M $K(NO)_3$, the reduction peak currents in all cases were found to be linearly proportional to the square root of the scan rates as shown in Supplementary material, Fig. S1. Based on the Randles–Sevcik equation $I_p = 2.69 \times 10^5\ n^{3/2} A D_0^{1/2} C_0 \nu^{1/2}$, the electroactive area A can be determined from the slope of a plot of the voltammetric peak current I_p versus the square root of scan rate $\nu^{1/2}$ (Ding et al., 2005). From the slopes of the three straight lines for the SP@AuNPs/MWNTs/GCE (curve a), SP@AuNPs/GCE (curve b) and bare GCE (curve c) sensors in Fig. S1, the electroactive surface areas of the corresponding electrodes are calculated to be 1.28 cm^2, 0.72 cm^2 and 0.14 cm^2, respectively. The SP@AuNPs/MWNTs/GCE nanocomposite electrode has a 9-fold increase in the electroactive surface area as compared to the bare GCE electrode. The increase in the electroactive surface area certainly will be favorable for achieving faster electron-transfer kinetics at the electrode interface and a high loading for the enzyme in the immobilization procedure, leading a more sensitive response to the analyte.

Electrochemical impedance spectra (EIS) were performed to provide further information on the morphology with respect to the interfacial electron-transfer kinetics. The impedance spectra of electrodes coated with SPs, SP@AuNPs, SP@AuNPs/MWCNTs, and the enzyme MPH immobilizing MPH/SP@AuNPs/MWCNTs are shown in Fig. 2. The impedance of the bare GCE was 323 Ω (Fig. 2a), and after treated with SP, the EIS of the SP/GCE had a slightly increase (405 Ω, Fig. 2b) due to the nonconductive property of SP. However, the SP@AuNPs coated GCE had a significant decrease in the resistance (218 Ω, Fig. 2c), and a further decrease in the resistance was observed for the SP@AuNPs/MWCNTs modified electrode (137 Ω, Fig. 2d). The combination of AuNPs and MWCNTs plays an important role in the electronic transport and is favorable for the charge exchange at the electrode interface, due to the presence

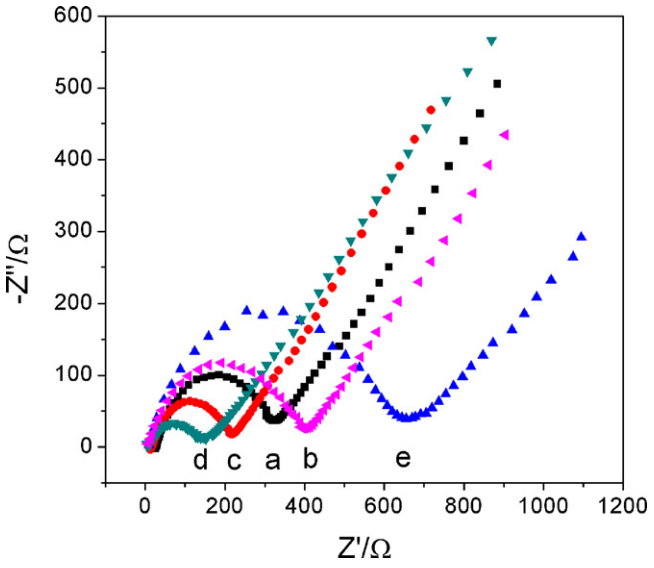

Fig. 2. Electrochemical impedance spectra in 10 mM $K_3Fe(CN)_6$ and $K_4Fe(CN)_6$ at the electrodes (a) bare GCE, (b) SP/GCE, (c) SP@AuNPs/GCE, (d) SP@AuNPs/MWNTs/GCE, and (e) MPH/SP@AuNPs/MWNTs/GCE.

of a synergistic effect in the SP@AuNPs/MWCNTs nanocomposite film. When the enzyme MPH was covalently immobilized onto the SP@AuNPs/MWCNTs/GCE surface, a remarkable increase in the interfacial resistance (671 Ω, Fig. 2e) was resulted, meaning the coverage of the protein on the nanocomposite surface.

3.3. Square wave voltammetry of the biosensor

The electrode process of 4-nitrophenol can be initiated from an irreversible multiple-step reduction of 4-nitrophenol to 4-aminophenol, then oxidized to quinoneimine on the return positive scan (Alizadeha et al., 2009). In the determination of methyl parathion, cyclic voltammetry was firstly applied to the biosensor MPH/SP@AuNPs/MWCNTs/GCE in the methyl parathion solution with 6 scan cycles in the region from −1.5 to +1.5 V. This process ensured the enzymatic hydrolysis of methyl parathion and conversion of the released 4-nitrophenol to 4-aminophenol. The oxidation current density from the conversion of 4-aminophenol to quinoneimine was related to the concentration of methyl parathion. As shown in Fig. 3, no redox peak was observed at MPH/SP@AuNPs/MWCNTs/GCE (curve a) in pH 7.0 PBS in the absence of methyl parathion. When 0.1 μg mL^{-1} methyl parathion was added into the PBS electrolyte, the SWV of the biosensor showed an oxidative peak at 589 mV (curve d), due to the oxidation of 4-aminophenol to quinonimine. Whereas in the cases of nanocomposite underlayers composed of SP@AuNPs and SPs/MWCNTs, respectively, the corresponding electrodes exhibited lower peak current responses (curve b and c).

According to the data from Fig. 3, the MPH/SP@AuNPs/MWCNTs/GCE biosensor gave a current response at methyl parathion concentration 0.1 μg mL^{-1} (curve d) with ~1.8- and ~3.1-fold increases as compared to the responses of the MPH/SP@AuNPs/GCE (curve c) and the MPH/SP/MWCNTs/GCE (curve b), respectively. The result implies the occurrence of a strong synergistic effect between the SP@AuNPs and MWCNTs particles, which enhances the charge exchange of the electrode process. The mechanism may stem from the fact that the composition of SP/AuNPs particles with MWCNTs can not only improve the specific surface area for a higher loading of the enzyme, but also increase the close contact area between the composite and the electrode surface. These SWV behaviors are consistent with the results from

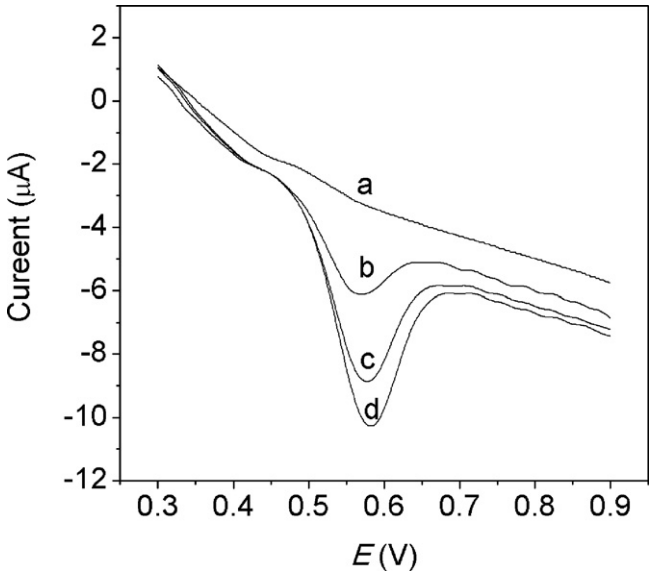

Fig. 3. The square wave voltammetric responses of (a) SP@AuNPs/MWNTs/GCE in pH 7.0 PBS, (b) MPH/SP@AuNPs/GCE, (c)MPH/SP/MWNTs/GCE and (d) MPH/SP@AuNPs/MWNTs/GCE in pH 7.0 PBS containing 0.1 μg mL^{-1} methyl parathion.

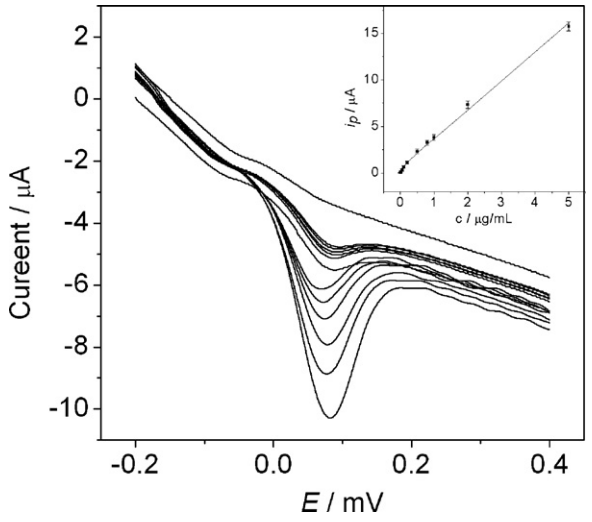

Fig. 4. The square wave voltammetric responses of the MPH/SP@AuNPs/MWNTs/GCE biosensor towards methyl parathion with varying concentrations. Inset: linear relationship between peak currents and methyl parathion concentrations.

the CV and EIS characterizations, as the SP@AuNPs/MWCNTs film possesses a lowest interfacial resistance.

3.4. Optimization of nanocomposite components

There are several reasons for choosing SPs, AuNPs and MWCNTs as the constituents for the formation of the nanocomposite. SPs have been extensively used in the fabrication of various biosensors as the entrapping layer because of the high specific surface area providing a high loading capacity for enzyme protein immobilization (Wang and Caruso, 2005). AuNPs as the shell of SP particle can provide the material with high conductivity. Moreover, the presence of AuNPs in the sensing film is beneficial to reduce the overpotential (Jena and Raj, 2006). Another feature is the biocompatibility of the nanostructure which has been proven to keep enzyme activity for a lengthened storage time (Rozenberg and Tenne, 2008).

The size effect of SPs on the sensitivity of the nanocomposite biosensor was firstly investigated. With the diameter increase from 50 nm to 450 nm, the MPH/SP@AuNPs/MWNTs/GCE biosensor produced a bell-shaped response curve with a maximum at the size diameter 100 nm (Supplementary material, Fig. S3a). SP with smaller or larger size resulted in lower responses. The effect of AuNPs content in the core–shell nanostructure on the response current was investigated by varying the volumetric ratio of applied AuNP solution to the SP suspension from 0 to 2, and a similar response curve centered at the volumetric ratio 1 was obtained (Supplementary material, Fig. S3b). The amount of MWCNTs has also an obvious influence on the biosensor behavior. With the increase of the amount of MWCNTs in the nanocomposite layer, the current gradually increased and reached a maximum at an applied final concentration 1.5 μg mL^{-1} (Supplementary material, Fig. S3c).

Through the above optimization procedure, optimal SP size and amounts of the components for the formation of a suitable nanocomposite were established. Under the optimized conditions, the optimized nanocomposite film exhibits the capacibility to improve the loading of the enzyme protein and the conductivity; therefore an enhanced synergistic effect can be produced in the biosensor performance. The optimization procedure is critical for the elaboration of a biosensor by utilizing nanocomposite.

3.5. Analytical performance

A biosensor with a good analytic performance is characterized by the high sensitivity (i.e., low detection limit), wide dynamic response region, and the utilizability in an interference environment. Fig. 4 displays the SWV responses of methyl parathion at different concentrations determined by the MPH/SP@AuNPs/MWNTs/GCE biosensor. The well-defined peaks reveal a nearly straight response line that is proportional to the methyl parathion concentrations in the range from 0.001 μg mL^{-1} to 5.0 μg mL^{-1} (Fig. 4, inset). The linear regression equation, I (μA) = 3.167 C + 0.345, can be established with a correlation coefficient of 0.9969. A detection limit of 0.3 ng mL^{-1} was obtained based on the signal-to-noise ratio equal to 3. The detection limit obtained is lower than that with GCE (Manisankar et al., 2006). The relative standard deviation was obtained to be 2.1% for ten replicated determinations of methyl parathion at the concentration of 0.1 μg mL^{-1}, indicating acceptable reproducibility. When the MPH/SP@AuNPs/MWNTs/GCE sensor was not in use, it can be stored at 4 °C under dry conditions, and no obvious deterioration in the response to the analyte was observed in the first 10-days of storage. After storage for 30 days the sensor still retained 80% of its initial current response.

The MPH/SP@AuNPs/MWNTs/GCE biosensor was tested for its selectivity against the methyl parathion analogs: ethyl parathion and paraoxon, at the same fixed concentration 1 μg mL^{-1} in PBS. Their responses together with that of methyl parathion are shown in Supplementary material Fig. S4, and ~9-fold and ~12.6-fold selectivities over the two analogs were observed. For the interference test, the inorganic salts at a final concentration of 0.5 mg mL^{-1} were separately introduced into methyl parathion solutions at 1 μg mL^{-1} in PBS, and no significant interference was observed (Supplementary material Fig. S4). The specificity for the determination of methyl parathion by using the nanocomposite biosensor stems from the nature of the immobilizing MPH enzyme. Another fact is the MPH protein cannot be easily denatured by the tested interference substances, and high activity can be maintained in the test environment.

The recovery rate test with known amounts of methyl parathion in garlic samples resulted the recovery rates in the range from 95.0% to 102.3% based on the average of a triplicate test at each concentration. The data are summarized in Table 1. The results indicate

Table 1
Recovery ratios of methyl parathion in spiked garlic samples.

Sample	Taken (ng mL^{-1})	Found (ng mL^{-1})	Recovery (%)	RSD (%)
1	1.00	0.95	95.0	3.4
2	10.0	9.8	98.0	6.3
3	50.0	50.6	101.2	5.4
4	200	204.5	102.3	6.7
5	5000	4896	97.9	6.9

that the proposed biosensor is highly accurate, precise and reproducible, and it can be used for the analysis of samples from a real environment.

4. Conclusion remarks

A protocol for the construction of a MPH enzyme biosensor is developed for the determination of methyl parathion. The biosensor is based on the covalent immobilization of methyl parathion hydrolase onto the SP@AuNPs/MWCNTs nanocomposite interface on GCE electrode. The use of this biosensor for the selective and sensitive determination of methyl parathion has been demonstrated through the performance evaluation and the applications in the analysis of standard and spiked samples. Several advantages can be derived from this work. The nanocomposite prepared under the optimal conditions benefits not only the increase of enzyme loading on the electrode surface, but also the promotion of the interfacial electron exchange in the electrode process. The performance of the SP@AuNPs/MWCNTs nanocomposite biosensor has been demonstrated to be improved greatly as compared with the electrodes modified by SP@AuNPs or SPs/MWCNTs particles alone, due to the notably synergistic effect in the biosensing of methyl parathion. The nanocomposite biosensor can be used for the determination of methyl parathion in samples from a real environment with appreciable selectivity and sensitivity. Moreover, the nanocomposite film may be used as a new promising tool extensible for the elaboration of other analyte specific enzyme biosensors.

Acknowledgments

The authors gratefully acknowledge the financial supports of the National Natural Science Foundation of China (Nos. 20972056, and 21075047) and the PCSIRT (No. IRT0953). This work is also partially supported by the Open Foundation Program from the Key Laboratory of Catalysis and Materials Science of the State Ethnic Affairs Commission and Ministry of Education, South-Central University for Nationalities. We also thank anonymous reviewers for scientific comments and suggestions on illustrations in our previous submission to this journal.

Appendix A. Supplementary data

Supplementary data associated with this article can be found, in the online version, at doi:10.1016/j.bios.2011.04.025.

References

Al-Otayk, S., El-Shinawy, M.Z., Motawei, M.I., 2008. JKAU: Met. Environ. Arid Land Agric. Sci. 20, 63–79.
Alizadeh, T., Ganjali, M.R., Norouzi, P., Zare, M., Zeraatkar, A., 2009. Talanta 79, 1197–1203.
Azadi, P., Farnood, R., Meier, E., 2010. J. Phys. Chem. A 114, 3962–3968.
Bakker, E., Qin, Y., 2006. Anal. Chem. 78, 3965–3984.
Chen, S.G., Yin, Y.S., Wang, D.P., Lin, J., 2004. J. Cryst. Growth 267, 100–109.
Choi, B.G., Park, H.S., Park, T.J., Yang, M.H., Kim, J.S., Jang, S.Y., Heo, N.S., Lee, S.Y., Kong, J., Hong, W.H., 2010. Nano 4, 2910–2918.
Cui, X.Q., Li, C.M., Zang, J.F., Zhou, Q., Gan, Y., Bao, H.F., Guo, J., Lee, V.S., Moochhala, S.M., 2007. J. Phys. Chem. C 111, 2025–2031.
Cui, Z.L., Li, S.P., Fu, G.P., 2001. Appl. Environ. Microbiol. 67, 4922–4925.
Ding, S.J., Chang, B.W., Wu, C.C., Lai, M.F., Chang, H.C., 2005. Anal. Chim. Acta 554, 43–51.
Du, D., Chen, W.J., Zhang, W.Y., Liu, D.L., Li, H.B., Lin, Y.H., 2010. Biosens. Bioelectron. 25, 1370–1375.
Du, D., Huang, X., Cai, J., Zhang, A.D., Ding, J.W., Chen, S.Z., 2007. Anal. Bioanal. Chem. 387, 1059–1065.
Dzyadevych, S.V., Alexey, P.S., Chovelon, J.M., 2002. Anal. Chim. Acta 459, 33–41.
Grimsley, J.K., Calamini, B., Wild, J.R., Mesecar, A.D., 2005. Arch. Biochem. 442, 169–179.
Hiramatsu, H., Osterloh, F.E., 2003. Langmuir 19, 7003–7011.
Hu, S.S., Xu, C.L., Wang, G.P., Cui, D.F., 2001. Talanta 54, 115–123.
Jena, B.K., Raj, C.R., 2006. Anal. Chem. 78, 6332–6339.
Kim, J.H., Bryan, W.W., Chung, H.W., Park, C.Y., Jacobson, A.J., Lee, T.R., 2009. Appl. Mater. Interfaces 1, 1063–1069.
Kumar Jena, Bikash, Retna Raj, C., 2006. Anal. Chem. 78, 6332–6339.
Kumar, J., Jha, S.K., D'Souza, S.F., 2006. Biosens. Bioelectron. 21, 2100–2105.
Lee, J.H., Park, J.Y., Min, K., Cha, H.J., Choi, S.S., Yoo, Y.J., 2010. Biosens. Bioelectron. 25, 1566–1570.
Li, F.H., Song, J.X., Li, F., Wang, X.D., Zhang, Q.X., Han, D.X., Ivaska, A., Niu, L., 2009. Biosens. Bioelectron. 25, 883–888.
Manisankar, P., Selvanathan, G., Vedhi, C., 2006. Talanta 68, 686–692.
Mulbry, W.W., Karns, J.S., 1989. J. Bacteriol. 171, 6740–6746.
Pedrosa, V.A., Paliwal, S., Balasubramanian, S., Nepal, D., Davis, V., Wild, J., Ramanculov, E., Simonian, A., 2010. Colloids Surf. B 77, 69–74.
Pividori, M.I., Alegret, S., 2010. Nanocomposites 8, 8139–8168.
Rozenberg, B.A., Tenne, R., 2008. Prog. Polym. Sci. 33, 40–112.
Stober, W., Fink, A., Bohn, E., 1968. J. Colloid Interface Sci. 26, 62–69.
Su, S., He, Y., Song, S.P., Li, D., Wang, L.H., Fan, C.H., Lee, S.T., 2010. Nanoscale 2, 1704–1707.
Vie, R., Azema, N., Quantin, J.C., Touraud, E., Fouletier, M., 2007. Colloids Surf. A: Physicochem. Eng. Aspects 298, 192–200.
Villatte, F., Schulze, H., Schmid, R.D., Bachmann, T.T., 2002. Anal. Bioanal. Chem. 372, 322–326.
Wang, Y.J., Caruso, F., 2005. Chem. Mater. 17, 953–961.
Xian, Y.Z., Hu, Y., Liu, F., Xian, Y., Wang, H.T., Jin, L.T., 2006. Biosens. Bioelectron. 21, 1996–2000.
Zhou, X., Xu, L., Wang, Y., Kuang, Q., Shi, Y.F., Zhong, L.B., Zhang, Q.Q., 2010. J. Phys. Chem. C 114, 19607–19613.